Chapter V

Tetranuclear Schiff base copper(II) complexes: Syntheses, crystal structure, DNA/protein binding and catecholase-like activity

---

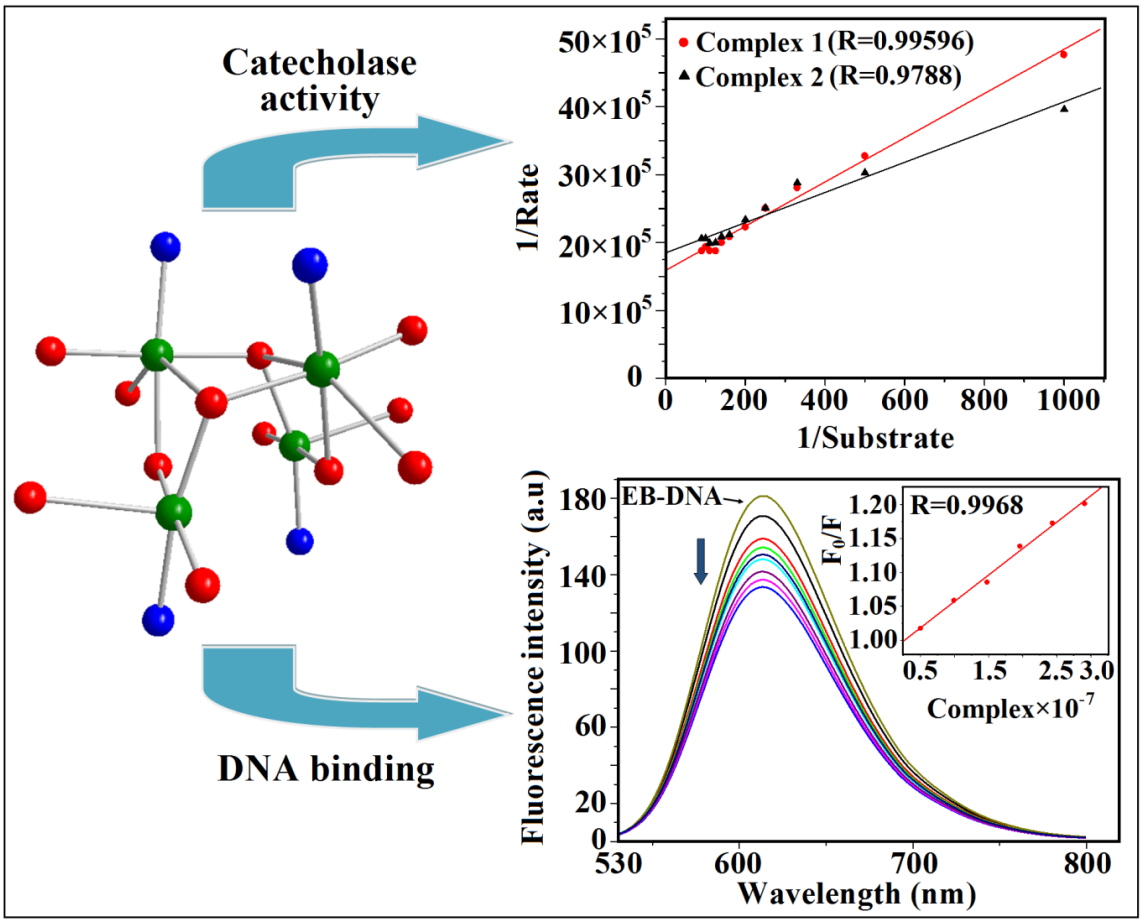

5.1. Introduction

Study of transition metal coordination compounds of Schiff base ligands has attracted interest in the last few decades, not only for their intriguing structures, but also for properties manifested in the fields of magnetism,[5.1] catalysis,[5.2] fluorescence,[5.3] medicinal chemistry,[5.4] etc. Among the 3d metal coordination compounds, polynuclear copper(II) complexes have attracted consideration for their potential biological applications due to their antimicrobial,[5.5] antifungal,[5.6] antidiabetic[5.7] and antitumor activities,[5.8,5.5a] the latter showing a relatively low toxicity in comparison to well-known platinum compounds.[5.9] Depending upon the Schiff base ligand used, the copper(II) compounds, which have been widely reported in the literature, can adopt various coordination numbers and geometries, such as square planar, square pyramidal, trigonal bipyramidal and distorted octahedral. Tetranuclear copper complexes with a large variety of structural motifs, such as cubane,[5.10] pin-wheel,[5.11] cyclic[5.12] and roof-shaped,[5.13] have been exploited with the aim to access correlations between their molecular structure and magnetic behavior. In the last decade several synthetic copper(II) compounds have been studied for developing new bioinspired catalysts.[5.14] In addition, multinuclear metal complexes have been anticipated as synthetic metallonucleases to catalyze the hydrolysis of phosphodiester bonds in DNA in order to develop novel metallopharmaceuticals.[5.15] For these purposes, studies of the interaction of copper complexes with CT-DNA and serum albumins using spectroscopic techniques represent a key point to develop possible copper metal based drugs.

Catechol oxidase, a copper enzyme with a type-3 active site, catalyzes the oxidation of a wide range of o-diphenols (catechols) to their quinones. The catalytic activity of copper complexes mimicking the catechol oxidase enzyme depends on many factors, such as coordination environment, metal–metal distance, type of bridging ligand etc.[5.14] A literature study reveals that several mononuclear and dinuclear copper(II) complexes have been

reported showing catecholase-like activity,[5.16] but there are only a limited number of copper(II) complexes of high nuclearity.[5.17]

In the present contribution, using the multidentate Schiff base ligand 2-[(2-hydroxy-ethylimino)-methyl]-6-methoxy-phenol) (H_2L), we have synthesized two tetranuclear copper(II) complexes, $[Cu_4(L)_2(LH)_2(H_2O)_2](ClO_4)_2 \cdot 3H_2O$ (**1**) and $[Cu_4(L)_2(LH)_2(H_2O)_2](ClO_4) \cdot (tp)_{0.5} \cdot 3H_2O$ (**2**) (tp = terephthalate), both comprising a double open cubane core structure. The interactions of complexes **1** and **2** with calf thymus DNA (CT-DNA), bovine (BSA) and human (HSA) serum albumin were studied using spectroscopic techniques. The catecholase activity of these complexes has also been investigated.

5.2. Experimental

5.2.1. Materials and physical measurements

Highly pure ethanolamine (98%) was purchased from Merck. Bovine serum albumin (BSA), human serum albumin (HSA), ethidium bromide (EB) and calf thymus DNA (CT-DNA) were purchased from Sigma Aldrich. All other reagent grade chemicals were commercially available and used as received. The solvents used for spectroscopic studies were purified and dried by standard procedures before use.[5.18]

Elemental analyses (carbon, hydrogen and nitrogen) were performed using a Perkin–Elmer 240C elemental analyzer. Electronic absorption spectra at room temperature were obtained with a Shimadzu UV-1601 UV–Vis spectrophotometer. Quartz cuvettes of 1 cm path length and 3 cm^3 volume were used for all measurements. IR spectra were recorded as KBr pellets on a Bruker Vector 22 FTIR spectrophotometer operating from 400 to 4000 cm^{-1}. Emission spectra were recorded on a Hitachi F-7000 spectrofluorimeter. The quantum yield was calculated according to the reported method.[5.19] The ESI-MS spectra of the compounds were

recorded in methanol with an Agilent Q-TOF 6500 mass spectrometer. A BAS Epsilon electrochemical analyzer was used for the cyclic voltammetric measurements.

5.2.2. Synthesis

Caution! Since perchlorate salts are potentially explosive, only small amounts of the materials should be handled with care.

Complexes **1** and **2** have been synthesized adopting the procedures indicated in Scheme 5.1.

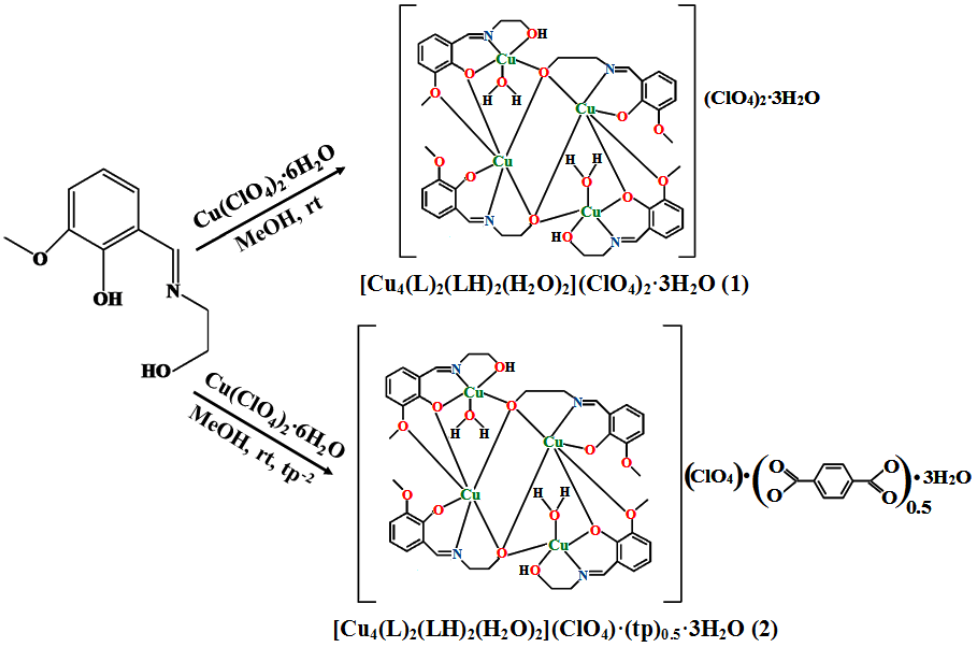

Scheme 5.1. Synthesis of complexes 1 and 2.

5.2.2.1. Synthesis of 2-[(2-hydroxy-ethylimino)-methyl]-6-methoxyphenol (H_2L)

The tridentate Schiff base 2-[(2-hydroxy-ethylimino)-methyl]-6-methoxy-phenol (H_2L) was prepared by the condensation reaction between 3-methoxysalicyldehyde (1 mmol, 0.152 g) and 2-aminoethanol (1 mmol, 0.06 g) in methanol (10 mL) according to the literature method.[5.20]

5.2.2.2. Synthesis of $[Cu_4(L)_2(LH)_2(H_2O)_2](ClO_4)_2 \cdot 3(H_2O)$ (1)

A methanolic solution (10 mL) of $Cu(ClO_4)_2 \cdot 6H_2O$ (0.5 mmol, 0.185 g) was added to a mixture of H_2L (0.5 mmol, 0.0976 g) and Et_3N (0.5 mmol, 0.05 g) in methanol under stirring

conditions. Stirring was continued for 2 h and then the reaction mixture was filtered. The green colored filtrate was left at room temperature and deep green crystals suitable for X-ray diffraction were obtained after a few days. Yield: 65%. *Anal.* Calc. for $C_{40}H_{56}Cl_2Cu_4N_4O_{25}$ (1317.95 g mol^{-1}): C, 36.45; H, 4.28; N, 4.25. Found: C, 36.43; H, 4.26; N, 4.28%.

5.2.2.3. $[Cu_4(L)_2(LH)_2(H_2O)_2](ClO_4)(tp)_{0.5}\cdot(H_2O)_3$ (2)

Complex **2** was synthesized following the procedure adopted for **1**, but using an additional methanolic solution (5 mL) of terephthalic acid (0.5 mmol, 0.83 g) and triethylamine (1 mmol, 0.101 g). The stirring was continued for 2 h, then the deep green color solution was filtered and the filtrate was kept at room temperature. After a few days deep green crystals suitable for X-ray diffraction were collected by filtration. Yield: 70%. *Anal.* Calc. for $C_{44}H_{57}ClCu_4N_4O_{22.50}$ (1291.55 g mol^{-1}): C, 40.91; H, 4.44; N, 4.33. Found: C, 40.89; H, 4.42; N, 4.35%.

5.2.3. Protein binding studies

Stock solutions of bovine serum albumin (BSA, 5.68 μM), human serum albumin (HSA, 1.85 μM) and the complexes (10 μM) were prepared in HEPES buffer solution (pH 7.2). The Stern–Volmer constant (K_{sv}) and quenching rate constant (k_q) were calculated using equations $F_0/F = 1 + K_{sv}[complex]$ and $K_{sv} = k_q\tau_0$, where F_0 and F are the fluorescence intensities in the absence and presence of the complex, and τ_0 is the lifetime of serum albumin (10^{-8} s). To calculate the binding constant of the compound with serum albumin, the Scatchard equation, $\log(F_o\text{-}F)/F = \log K_b + n \log[complex]$, has been used, where K_b is the binding constant of the compound with serum albumin and n is the number of binding sites per albumin.

5.2.4. DNA binding experiments

5.2.4.1. Electronic absorption spectral study

The interaction between the copper complexes and CT-DNA was investigated using UV–Vis absorption spectral studies at room temperature. For both complexes the interaction has been evaluated by the gradual addition of a 10 μL solution (6.66 μM) of CTDNA to a fixed concentration of the copper(II) complex (2 ml, 0.19 μM) in water. The intrinsic binding constant (K_{ib}) of the complexes with CT-DNA was determined using the equation:

$$\frac{[DNA]}{(\varepsilon_a - \varepsilon_f)} = \frac{[DNA]}{(\varepsilon_b - \varepsilon_f)} + \frac{1}{K_{ib}(\varepsilon_b - \varepsilon_f)}$$

Where CT-DNA concentration is represented by [DNA] and at a given CT-DNA concentration the extinction coefficient value of the complex is ε_a. The extinction coefficients of the free complex in solution is ε_f and when fully bound to CT-DNA is ε_b. The plot of [DNA]/($\varepsilon_a - \varepsilon_f$) vs [DNA] gives a straight line with $\frac{1}{(\varepsilon_b - \varepsilon_f)}$ and $\frac{1}{K_{ib}(\varepsilon_b - \varepsilon_f)}$ as the slope and intercept, respectively. The value of K_{ib} was calculated from the ratio of the slope to the intercept.

5.2.4.2. Competitive EB–DNA binding fluorescence measurement

The competitive binding nature of ethidium bromide (EB) and the metal complex with CT-DNA was investigated adopting a fluorometric method using an aqueous solution of EB bound CT-DNA in HEPES buffer at room temperature. The fluorescence intensities at 614 nm (λ_{ex}, 500 nm) of EB bound CT-DNA with increasing concentrations of the complex were recorded. The quenching constants (Stern–Volmer constant, K_{sv}) were calculated using the Stern–Volmer equation, $F_0/F = 1 + K_{sv}[complex]$, where F_0 and F are the emission intensities in the absence and presence of the copper(II) compound, K_{sv} is the Stern–Volmer constant and [complex] is the copper(II) complex concentration.

5.2.5. Crystallographic data collection and refinement

Data collections for complexes **1** and **2** were carried out at 120 K with Mo Kα radiation (λ = 0.71073 Å) on an Xcalibur diffractometer equipped with a Sapphire 3CCD camera. Cell

refinement, indexing and scaling of the data sets were done by using program CRYSALISPRO.[5.21] The structures were solved by direct methods and subsequent Fourier analyses,[5.22] and then refined by the full-matrix least squares method based on F^2 with all observed reflections.[5.22] In **2**, the perchlorate oxygen atoms and one water molecule were refined over two disordered positions (occupancies of 0.598(9)/0.402(9) and 0.59(3)/0.41(3), respectively). An additional residue was interpreted as a water molecule with half occupancy. All the calculations were performed using the WINGX System, Ver 1.80.05.[5.23] The molecular structures were obtained with the graphical program DIAMOND.[5.24] Crystal data and details of the refinements are given in Table 5.1.

Table 5.1. Crystal data and details of structure refinement of complexes 1 and 2.

Complex	1	2
Empirical formula	$C_{40}H_{56}Cl_2Cu_4N_4O_{25}$	$C_{44}H_{57}ClCu_4N_4O_{22.50}$
Formula mass (g mol^{-1})	1317.95	1291.55
Crystal system	Monoclinic	Monoclinic
Space group	$P2_1/c$	$P2_1/n$
a (Å)	11.8650(6)	14.6377(3)
b (Å)	23.6691(7)	21.7677(5)
c (Å)	18.4922(8)	16.8163(4)
β (°)	98.048(4)	108.225(2)
V (Å^3)	5142.1(4)	5089.4(2)
Z	4	4
D_{calcd} (g cm^{-3})	1.702	1.686
μ(Mo-Kα) (mm^{-1})	1.825	1.788
F(000)	2696	2648
θ range (°)	3.11 - 26.02	2.55 - 28.28
No. of collected data	44411	62449
No. of unique data	10110	12525
R_{int}	0.0849	0.0599
Observed reflns [I> 2σ(I)]	7502	9269
Goodness of fit (F^2)	1.188	1.037
Parameters refined	692	729
R_1, wR_2 (I >2σ(I)) [a]	0.0772, 0.1549	0.0583, 0.1232
Residuals, e Å^{-3}	0.837, –0.767	0.908, –0.752

[a] $R_1(Fo) = \Sigma \left| |Fo| - |Fc| \right| / \Sigma |Fo|$, $wR_2(Fo^2) = [\Sigma w (Fo^2 - Fc^2)^2 / \Sigma w (Fo^2)^2]^{1/2}$

5.3. Result and discussion

5.3.1. Crystal structure description

The single crystal X-ray structure determination shows that both complexes **1** and **2** are comprised of structurally similar tetranuclear cationic species, $[Cu_4(L)_2(HL)_2(H_2O)_2]^{2+}$ (Figure 5.1), which are counterbalanced by two perchlorate anions in **1**, and perchlorate with terephthalate anions in **2**. Selected bond distances for the complexes are listed in Table 5.2. As the tetranuclear cations are similar, the description is limited to complex **1**. The cubane-like Cu_4O_4 core is formed by four copper atoms and four oxygen donors from four Schiff base ligands, two of which are deprotonated $[HL]^-$, acting as μ_2-η^1:η^1:η^2:η^1-O,N,O,O, the other di-deprotonated $[L]^{2-}$, acting as μ_3–η^1:η^1:η^3-O,N,O, and the overall geometry can be described as an open cage. In both of these complexes the four Cu(II) atoms are not crystallographically equivalent, although the species present a pseudo-two fold axis. The Cu1 and Cu3 copper centres exhibit a square pyramidal geometry, being chelated by imino nitrogen, phenoxido and alcoholic oxygen atoms (N1a/N1b, O2a/O2b, O1a/O1b for Cu1/Cu3, respectively) from two $[HL]^-$ ligands. The metals complete the basal plane with the alkoxido oxygen atoms from two $[L]^{2-}$ ligands. The apical position of the square pyramidal geometry at the Cu1 and Cu3 atoms is occupied by a water molecule (O1w and O3w). On the other hand, the Cu2 and Cu4 atoms present an octahedral coordination geometry formed by imino nitrogen, phenoxido and alkoxido oxygen atoms (N1c/N1d, O2c/O2d, O1c/O1d for Cu2/Cu4, respectively) from the ligands $[L]^{2-}$. The coordination sphere is completed by phenoxo O2a and O2b donors from the ligands $[HL]^-$ and at axial positions by another alkoxido atom, O1d/O1c, and the methoxy oxygen atom, O3a/O3b, for Cu2/Cu4, respectively.

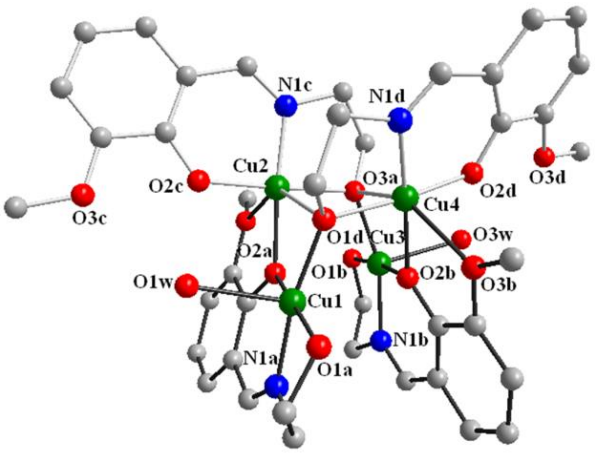

Figure 5.1. Molecular structure of complex 2 with labels of hetero-atoms. The same scheme applies also to complex 1.

Table 5.2. Selected bond lengths (Å) and intermetallic distances for complexes 1 and 2.

	1	2
Cu(1)-N(1a)	1.926(7)	1.946(4)
Cu(1)-O(1a)	2.048(5)	2.003(3)
Cu(1)-O(2a)	1.949(5)	1.957(3)
Cu(1)-O(1d)	1.923(5)	1.923(3)
Cu(1)-O(1w)	2.235(5)	2.290(3)
Cu(2)-N(1c)	1.922(7)	1.932(4)
Cu(2)-O(1c)	1.962(5)	1.954(3)
Cu(2)-O(2c)	1.919(5)	1.901(3)
Cu(2)-O(2a)	2.025(5)	1.995(3)
Cu(2)-O(3a)	2.432(5)	2.428(3)
Cu(2)-O(1d)	2.488(5)	2.532(3)
Cu(3)-N(1b)	1.937(6)	1.941(4)
Cu(3)-O(1b)	2.007(5)	1.994(3)
Cu(3)-O(1c)	1.910(5)	1.932(3)
Cu(3)-O(2b)	1.951(5)	1.946(3)
Cu(3)-O(3w)	2.262(5)	2.287(3)
Cu(4)-N(1d)	1.930(6)	1.934(4)
Cu(4)-O(1d)	1.987(5)	1.957(3)
Cu(4)-O(2d)	1.900(5)	1.896(3)
Cu(4)-O(2b)	1.996(5)	1.996(3)
Cu(4)-O(3b)	2.416(5)	2.432(3)
Cu(4)-O(1c)	2.554(5)	2.434(3)
Cu(1)-Cu(2)	3.2030(13)	3.1814(7)
Cu(1)-Cu(3)	3.9033(13)	3.8058(7)
Cu(1)-Cu(4)	3.2885(12)	3.3507(7)
Cu(2)-Cu(3)	3.3046(12)	3.2862(7)
Cu(2)-Cu(4)	3.3565(12)	3.2344(7)
Cu(3)-Cu(4)	3.1605(12)	3.1587(7)

The basal coordination bond distances (Table 5.2) for the Cu1 and Cu3 atoms are between 1.910(5) and 2.048(5) Å, while the aqua ligand at the apical position is somewhat more distant, at 2.235 (5) and 2.262(5) Å, respectively. The Addison parameter τ values[5.25] for the Cu1 and Cu3 centres [0.235 and 0.121] indicate that the penta-coordination geometry is square pyramidal. The degree of trigonality, τ, defined as (β-α)/60 (where β and α are the two largest coordination bond angles), is zero for a perfect square pyramidal, while it becomes unity for ideal trigonal bipyramidal geometry.The equatorial bond distances for the Cu2 and Cu4 centres are in the range 1.900(5)–2.025(5) Å, and as expected, the axial bond lengths, between 2.416(5) and 2.554(5) Å, are longer than the equatorial bond values, due to Jahn–Teller distortion. In addition, with the aim to outline the architecture of the cation, it is worth noting the rather long Cu1-O2b and Cu3-O2a distances of 2.878 and 2.891 Å, respectively.

The data of Table 5.2 indicate comparable values of the distances (most within their e.s.d.'s) for complexes **1** and **2**, but the Cu1 and Cu3 atoms in the latter show minor deviations from an ideal square pyramidal geometry, the τ parameters being 0.040 and 0.215, respectively.

In the crystal packing lattice water molecules with perchlorate ions (compound **1**, Figure 5.2) and lattice water molecules with terephthalate ions (in **2**, Figure 5.3) form layers through extended H-bonding that, via additional hydrogen bond interactions with the complex cations, give rise to a 3D network in both compounds.

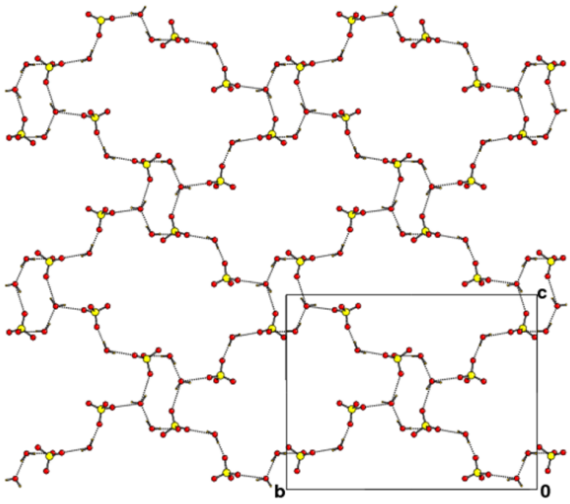

Figure 5.2. Layered structure in crystal packing of complex 1 formed by ClO_4 anions and water molecules connected by H-bonds.

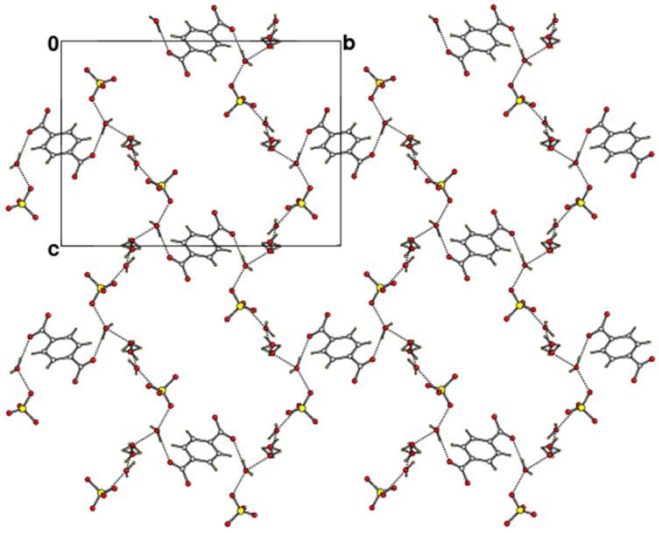

Figure 5.3. Layered structure in crystal packing of compound 2 formed by terephthalate anions and water molecules connected by H-bonds.

5.3.2. Electronic and emission spectra of complexes 1 and 2

The electronic spectra of complexes **1** and **2** were recorded in methanol (Figure 5.4**).** Compound **1** shows significant transitions at 235 nm ($\varepsilon \sim 8.11\times10^6$ L mol^{-1} cm^{-1}), 276 nm ($\varepsilon \sim 4.11\times10^6$ L mol^{-1} cm^{-1}) and 372 nm ($\varepsilon \sim 1.02\times10^6$ L mol^{-1} cm^{-1}), and the spectral transitions of compound **2** are at 212 nm ($\varepsilon \sim 7.75\times10^6$ L mol^{-1} cm^{-1}), 233 nm ($\varepsilon \sim 8.47\times10^6$ L mol^{-1} cm^{-1}), 271 nm ($\varepsilon \sim 3.33\times10^6$ L mol^{-1} cm^{-1}) and 373 nm ($\varepsilon \sim 2.42\times10^5$ L mol^{-1} cm^{-1}).

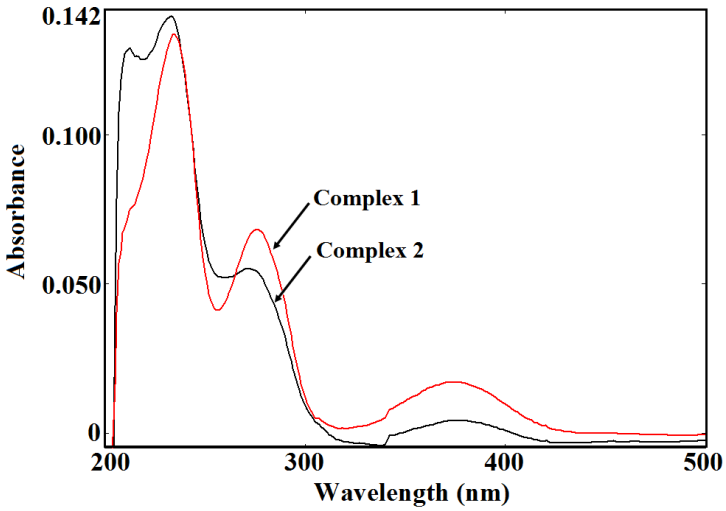

Figure 5.4. Electronic spectra of complexes 1 and 2 in methanol.

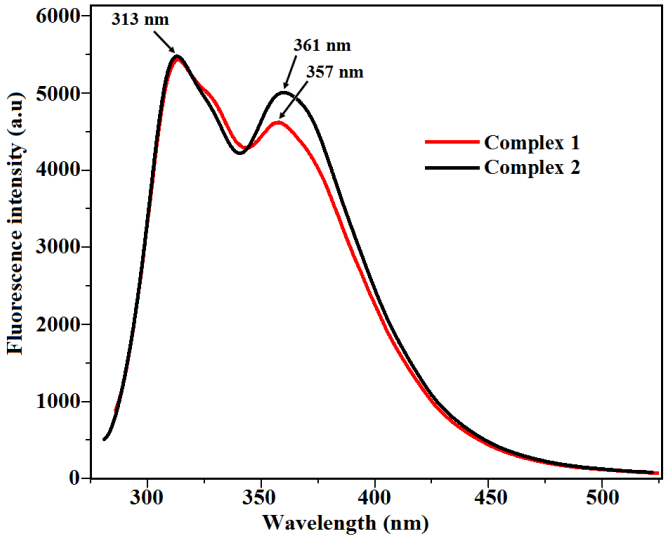

Figure 5.5. Fluorescence spectra of complexes 1 and 2 in methanol.

On excitation at 276 nm, compound **1** exhibits emission bands at 357 and 313 nm in methanol at room temperature and for compound **2** excitation at 271 nm results in emission bands at 361 and 313 nm (Figure 5.5).

5.3.3. Infrared spectra of complexes 1 and 2

The IR spectra show broad bands at around 3425 cm^{-1} for complex **1** and 3415 cm^{-1} for complex **2**, assigned to the ν(OH) stretching vibration of the lattice water molecules (Figure 5.6). In addition, bands at 513 and 817 cm^{-1} for complex **1**, and 509 and 814 cm^{-1} for **2**

indicate the presence of coordinated water molecules.[5.26] The bands at 1416 (for **1**) and 1429 cm^{-1} (for **2**) are due to the azomethine (C=N) group. The sharp peaks at 1079 (for **1**) and 1076 cm^{-1} (for **2**) give evidence for the presence of free perchlorate ions.[5.26] The bands at 2979 cm^{-1} for **1** and 2972 cm^{-1} for **2** are due to aromatic C-H stretching vibrations, and the bands at 2940 cm^{-1} for both compounds correspond to aliphatic ν(C-H) vibrations. Bands at 1165 and 1215 cm^{-1} for **1** and **2**, respectively, are assigned to $\nu(O\text{-}CH_3)$ vibrations. For **2**, the stretching frequencies of the free carboxylate ion, $\nu_a(CO_2^-)$ and $\nu_s(CO_2^-)$, appear at 1561 and 1467 cm^{-1}, respectively.

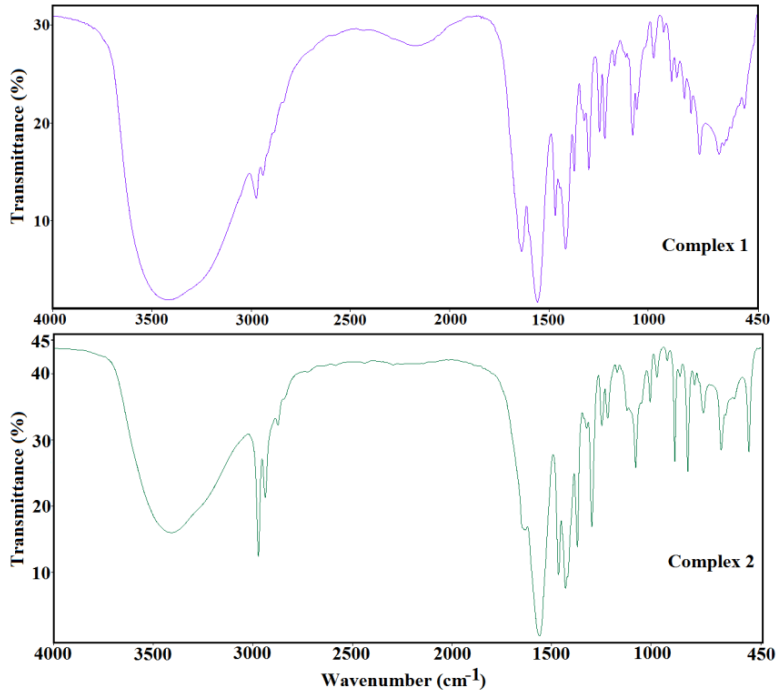

Figure 5.6. IR spectra of complexes 1 and 2.

5.3.4. ESI-MS spectra of complexes 1 and 2

The ESI mass spectra (Figures 5.7 and 5.8) of complexes **1** and **2** were recorded in methanol. The mass spectra show peaks at m/z = 1065.82 (Calc. 1066.03) and 1065.90 (Calc. 1066.03) for complexes **1** and **2**, respectively. These peaks correspond to the species $[C_{40}H_{48}N_4O_{14}Cu_4]$ $+H^+$ [Calc. m/z = 1064.02], clearly indicating that the tetranuclear composition of complexes is maintained in methanolic solution.

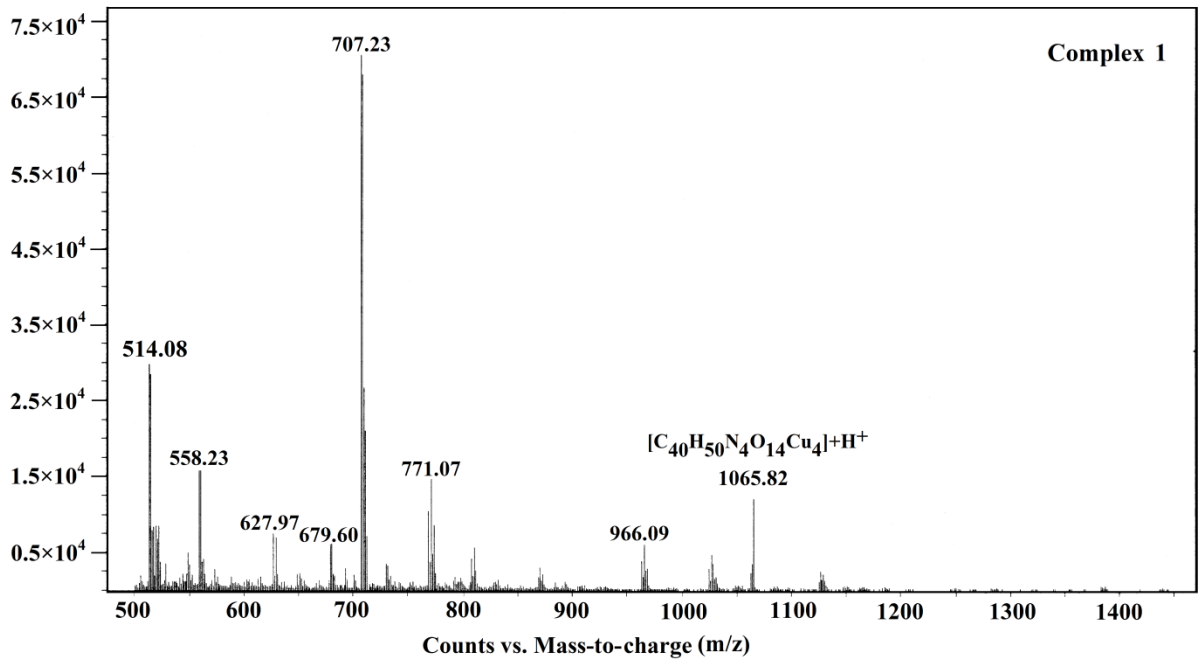

Figure 5.7. ESI- MS spectrum of complex 1 (recorded in methanol).

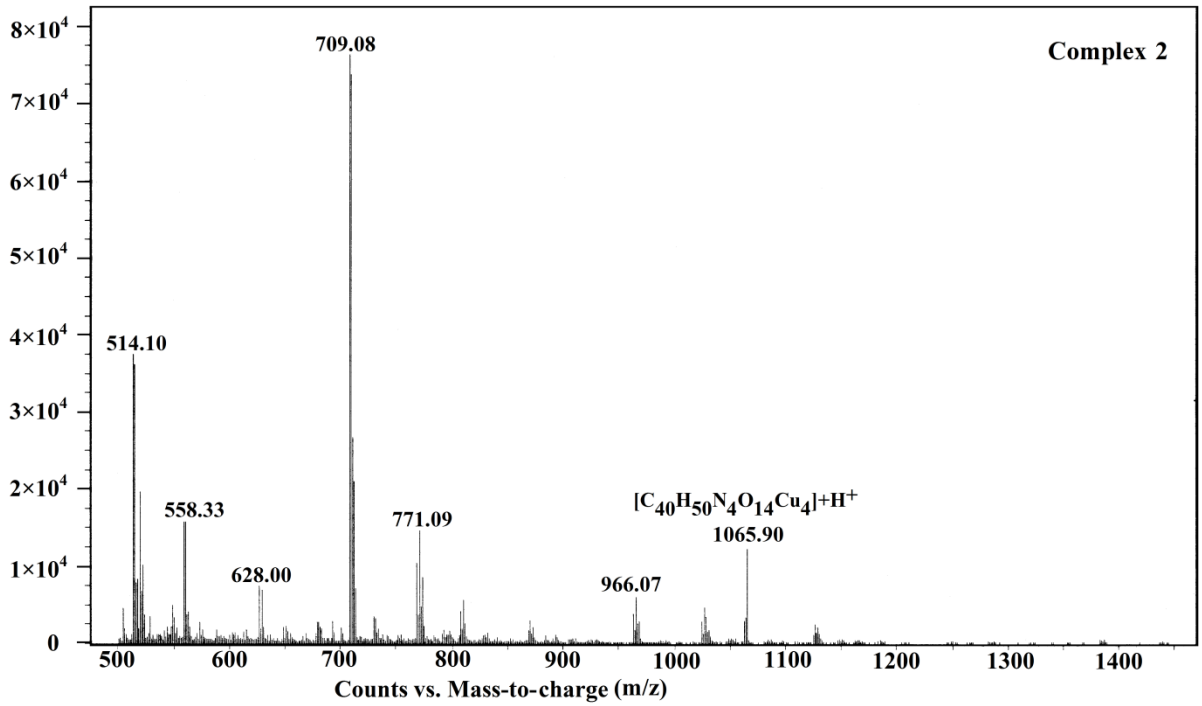

Figure 5.8. ESI- MS spectrum of complex 2 (recorded in methanol).

5.3.5. Catechol oxidase studies of complexes 1 and 2

3,5-Di-tert-butylcatechol (3,5-DTBC) is generally used as substrate to evaluate the catecholase activity of coordination compounds since the oxidation product, 3,5-di-tert-

butylquinone (3,5-DTBQ), is highly stable and gives a characteristic absorption band at 400 nm (ε= 1900 $M^{-1}cm^{-1}$) in methanol. To verify the catecholase-like activity of complexes **1** and **2**, a 10^{-4} M solution of each complex was treated with a 100-fold concentrated solution of 3,5-DTBC and the reaction was followed by recording the UV–Vis spectra of the mixture under aerobic conditions at intervals of 5 min up to 90 min. These spectral changes, after mixing 3,5-DTBC with complexes **1** and **2**, are shown in Figures 5.9 and 5.10, respectively.

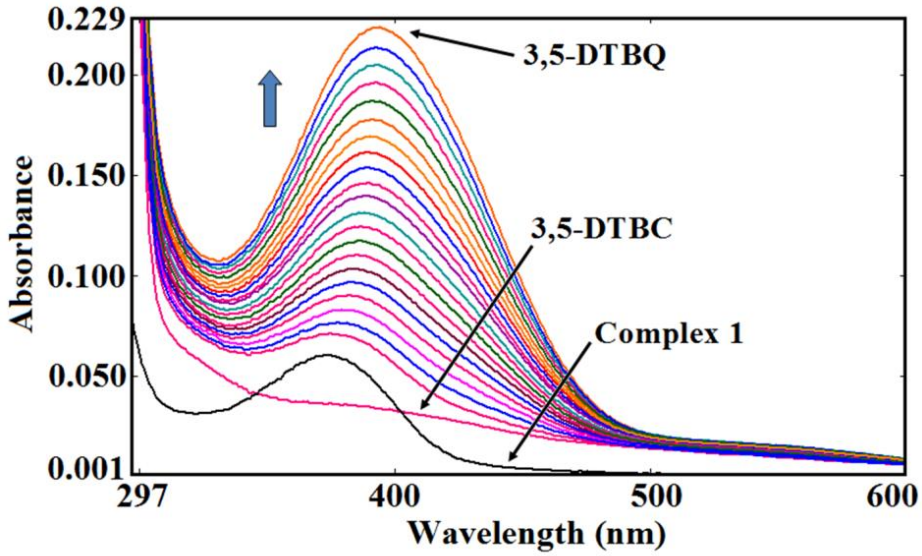

Figure 5.9. Increase of absorbance around 400 nm after the addition of 100 equiv of 3,5-DTBC to a methanolic solution of complex 1. The spectra were recorded at intervals of 5 min.

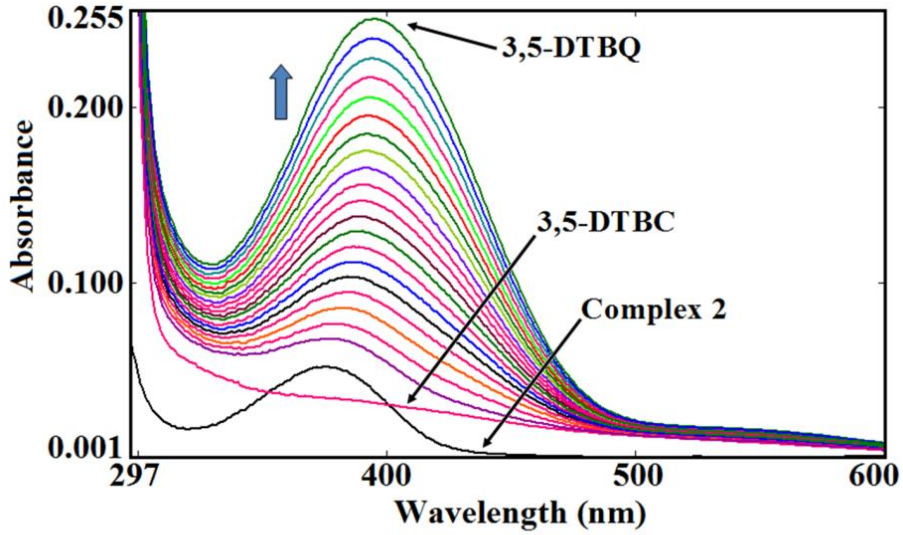

Figure 5.10. Increase in the absorbance around 400 nm after the addition of 100 equiv of 3, 5-DTBC to a methanolic solution of complex 2. The spectra were recorded at intervals of 5 min.

The rate constant was determined from the optical density versus time plot using the initial rate method [Figures 5.11 and 5.12]. The change of the rate of reaction with the concentration of substrate is shown in Figure 5.13, which allows the evaluation that at a low concentration of 3,5-DTBC the reaction rate is first order, whereas saturation kinetics are observed at higher concentrations.

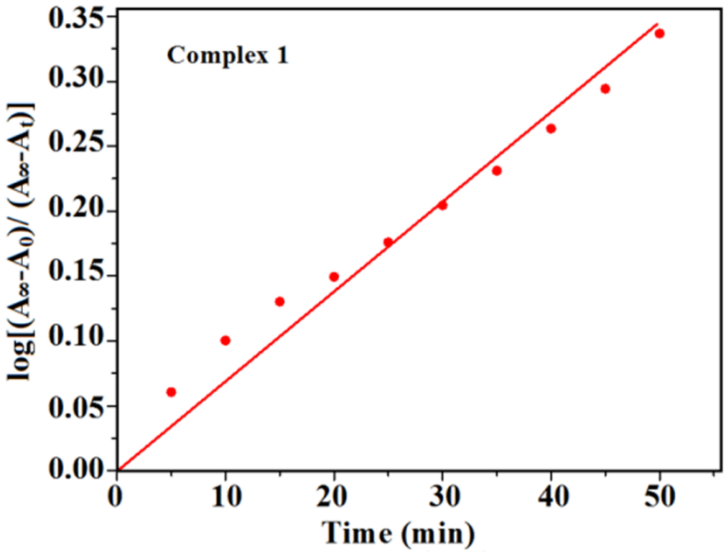

Figure 5.11. Plot of $\log(A_\infty - A_0)/(A_\infty - A_t)$ vs time with complex 1 as catalyst for the oxidation of 3,5-DTBC to 3,5-DTBQ.

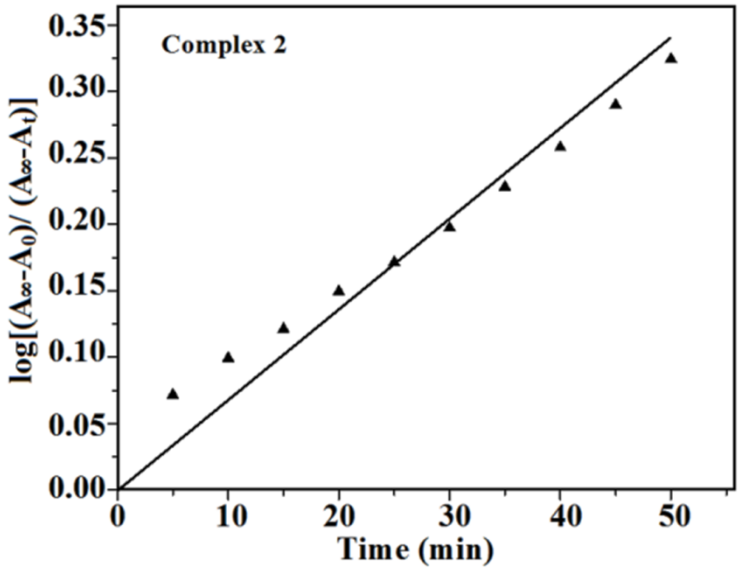

Figure 5.12. Plot of $\log(A_\infty - A_0)/(A_\infty - A_t)$ vs time with complex 2 as catalyst for the oxidation of 3,5-DTBC to 3,5-DTBQ.

The rate versus concentration of the substrate (Figure 5.13) was then analyzed on the basis of the Michaelis–Menten approach of enzymatic kinetics to get a Lineweaver–Burk plot (Figure 5.14), as well as the parameter values of the maximum initial rate (V_{max}), Michaelis–Menten constant (K_M) and turnover number (K_{cat}) (Table 5.3). Compound **1** showed a higher catecholase-like activity (k_{cat} = 113 h^{-1}) with respect to compound **2** (k_{cat} = 97 h^{-1}), which may be tentatively be referred to the larger distortions detected in the coordination geometry of the former complex [trigonality τ values of 0.235 and 0.121 for complex **1** and 0.040 and 0.215 for **2**], or to the templating effects of the counter ions. k_{cat}(hr^{-1}) for the catechol oxidation reaction of compounds **1** and **2** and of previously reported tetranuclear Cu^{II} complexes[5.27] by using 3,5-DTBC as substrate are given in Table 5.4.

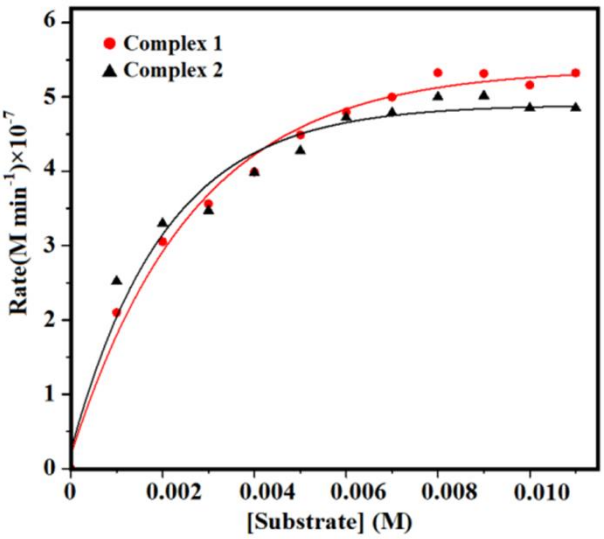

Figure 5.13. Initial rates *vs* substrate concentration for the 3,5-DTBC to 3,5-DTBQ oxidation reaction catalyzed by complexes 1 and 2 in methanol.

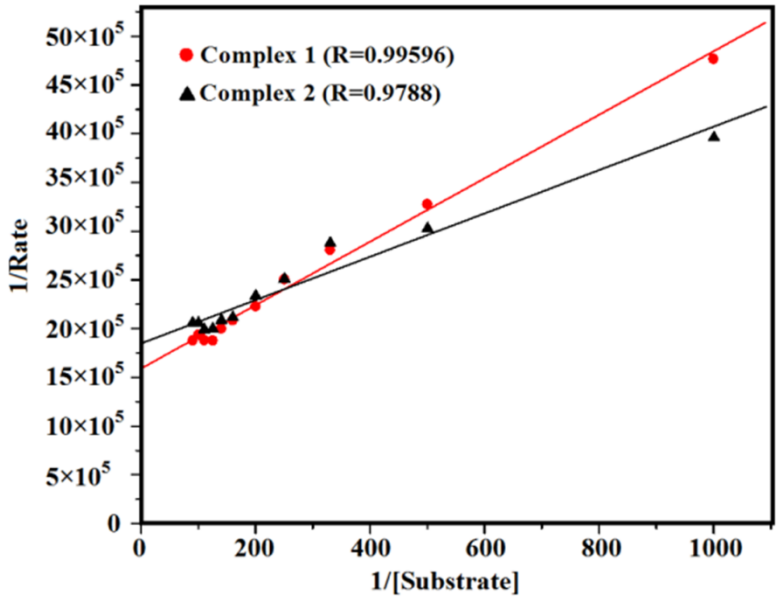

Figure 5.14. Lineweaver- Burk plot of complexes 1 and 2.

Table 5.3. Kinetics parameters for the catecholase activities of complexes 1 and 2 in methanol.

Complex	V_{max} (M min^{-1})	K_M(M)	K_{cat} (h^{-1})
1	6.289×10^{-7}	2.045×10^{-3}	113
2	5.406×10^{-7}	1.202×10^{-3}	97

Table 5.4. $k_{cat}(hr^{-1})$ **for the catechol oxidation reaction of compounds 1 and 2 and of previously reported tetranuclear** Cu^{II} **complexes by using 3,5-DTBC as substrate.**

Complex	Bridging	Solvent	$k_{cat}(hr^{-1})$	Ref.
$[Cu_4(L)_2(LH)_2(H_2O)_2](ClO_4)_2.3H_2O$	μ_3-oxo, μ-Oph	Methanol	113	This work
$[Cu_4(L)_2(LH)_2(H_2O)_2](ClO_4)(tp)_{0.5}.3H_2O$	μ_3-oxo, μ-Oph	Methanol	97	This work
$[Cu_4(L^1)(\mu OH)_2(H_2O)_4]\cdot 5H_2O$	μ-OH	MeCN/ H_2O	288	5.27a
$[Cu_4(L^2)_4(MeOH)_2(ClO_4)_2]$	μ-Oph	MeCN	162	5.27b
$[Cu_4(L^3)(\mu\text{-}O)(OAc)_4]$	μ-OPh, μ_4-oxo	MeCN - H_2O	78.48	5.27c
$[Cu_4(L^4)(OH)_4(Cl)_2](PF_6)_2$	μ-OH	CH_2Cl_2	2.16	5.27d
$[Cu_4(O)(L^5)_2(Ac)_4]$	μ_4-oxo	DMSO	-	5.27e

HL^1 = H_6Valbiim·$9H_2O$, HL^2 = 4-bromo-2-[(2-hydroxy-1,1-dimethyl-ethylamino)-methyl]-phenol, HL^3 = 2,6-bis[bis(2-methoxyethyl)aminomethyl]-4-methylphenol, L^4 = $X_6Me_3Imme_3$ (calix[6]arene N-ligand), HL^5 = 2,6-bis(2-thiophenemethylimino-methyl)-4-methylphenol .

In order to elucidate the mechanism and possible complex-substrate intermediate, we have recorded the ESI-MS spectra of 1:100 mixture of each complex with 3,5-DTBC (Figures 5.15 and 5.16). The peaks at m/z = 196.22 (for **1**) and 196.21 (for **2**) are due to protonation of the ligand $[H_2L]+H^+$. The formation of a complex–substrate intermediate species was identified by peaks at m/z = 477.50 (for **1**) and 477.44 (for **2**).[5.17] The peak at m/z = 243 can be assigned to the sodium–quinone aggregate $[3,5\text{-DTBQ}]+Na^+$. The molecular oxygen oxidising 3,5-DTBC to 3,5-DTBQ in this process is converted to H_2O_2, the formation of which is confirmed by the blue color observed when starch and potassium iodide are added to the mixture of the complex and 3,5-DTBC. It is interesting to note that such coloration is not observed in the absence of the complex. A probable mechanistic path for the formation of H_2O_2 as a by-product during the oxidation of 3,5-DTBC to 3,5-DTBQ catalyzed by a

copper(II) compound was suggested by Chyn and Urbach.[5.28] Based on the ESI-MS spectra and considering the formation of H_2O_2 as a by-product we have proposed a possible mechanism of the reaction, shown in Scheme 5.2. The catalytic reaction starts with the formation of intermediate I, then one copper centre acquires one electron from 3,5-DTBC to form the intermediate II [m/z = 477.50 (for **1**) and 477.44 (for **2**)].

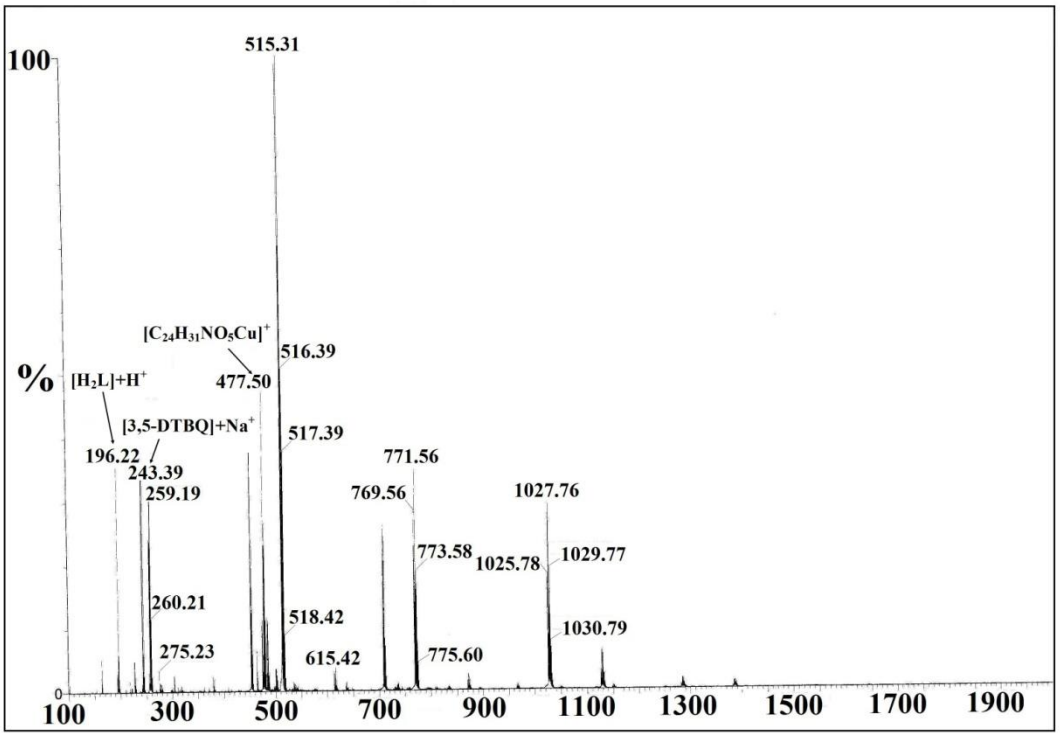

Figure 5.15. ESI-MS spectrum in methanol of the 1:100 mixture of complex 1 and 3,5-DTBC.

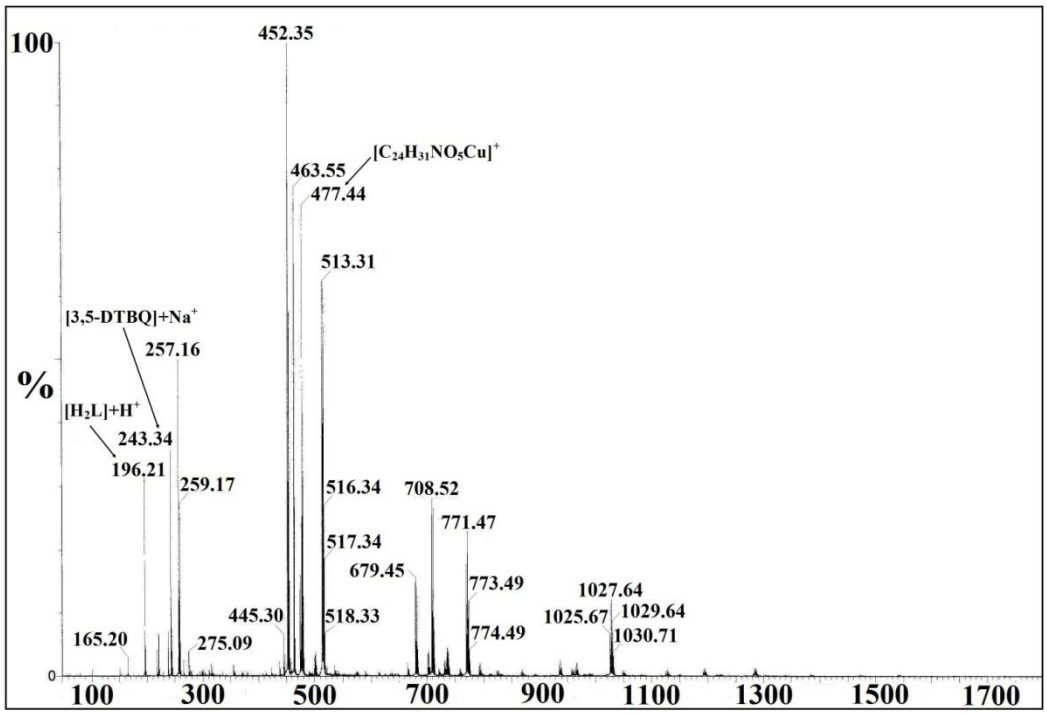

Figure 5.16. ESI-MS spectrum in methanol of the 1:100 mixture of complex 2 and 3,5-DTBC.

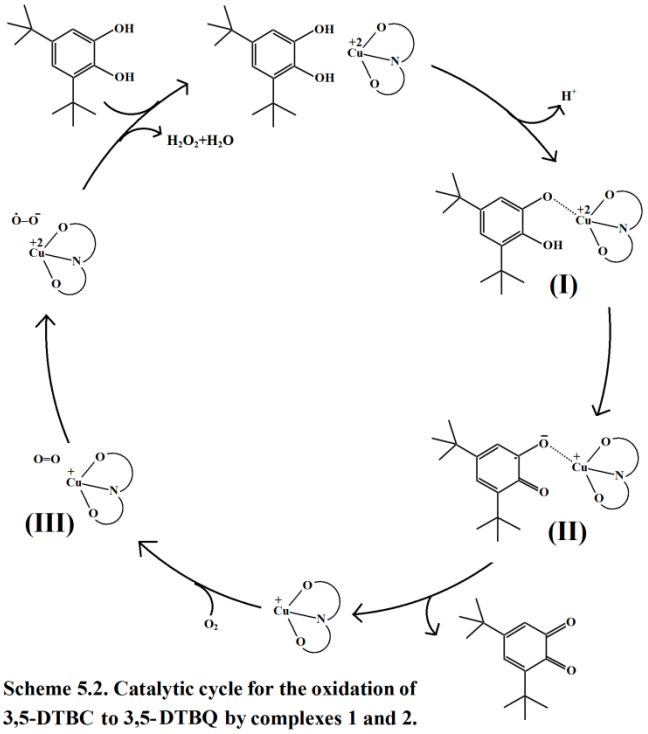

Scheme 5.2. Catalytic cycle for the oxidation of 3,5-DTBC to 3,5-DTBQ by complexes 1 and 2.

5.3.6. Protein binding studies

In a fluorometric study, 10 μL of an aqueous complex solution (10 μM) were gradually added to 3 ml of serum albumin solutions (BSA, 5.68 μM; HSA, 1.85 μM) and the quenching of the

emission intensities at 340 nm (λ_{ex}, 278 nm) for BSA and at 330 nm(λ_{ex}, 278 nm) for HSA was recorded. Upon gradually increasing the complex concentration, the fluorescence intensity of BSA and HSA significantly decreased (Figures 5.17–5.18 and 5.19–5.20). The K_{sv} values were calculated using the Stern–Volmer plot (Figure 5.21 for BSA, and Figure 5.22 for HSA). The calculated binding constants (k_b) for the interaction of the complex with the serum albumins are (4.21×10^7) ± 3.74 L mol^{-1} (**1**–BSA), (8.53×10^3) ± 1.90 L mol^{-1} (**1**–HSA), (2.46×10^6) ± 2.31 L mol^{-1} (**2**–BSA) and (8.25×10^3) ± 2.76 L mol^{-1} (**2**–HSA) (Table 5.5).

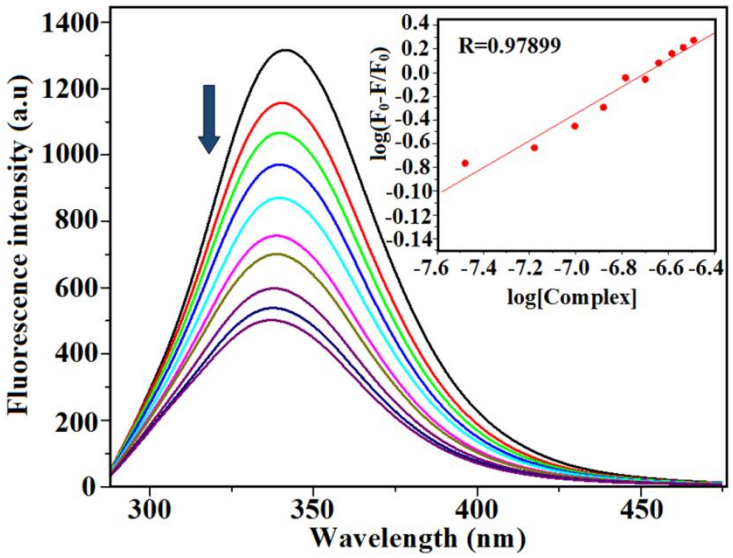

Figure 5.17. Change of the emission spectra of BSA (3 ml, 5.68 µM aqueous solution) upon gradual addition of 10 µL of an aqueous solution (10 µM) of complex 1 at room temperature. The arrow indicates the increase of the complex concentration.

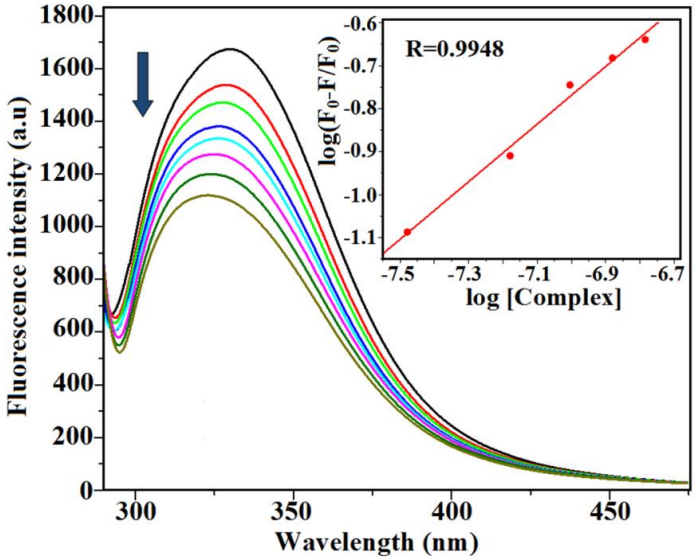

Figure 5.18. Change of the emission spectra of HSA (3 ml, 1.53 µM aqueous solution) upon gradual addition of 10 µL of an aqueous solution (10 µM) of complex 1 at room temperature. The arrow indicates the increase of the complex concentration.

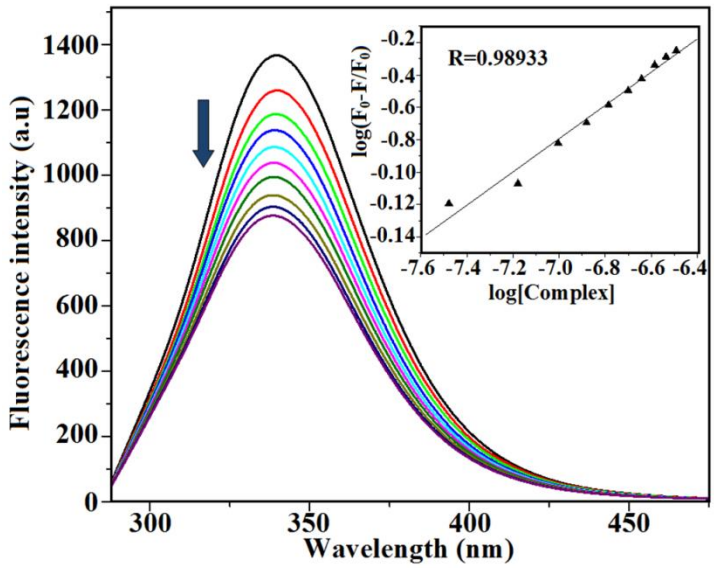

Figure 5.19. Change of the emission spectra of BSA (3 ml, 5.68 µM aqueous solution) upon gradual addition of 10 µL of an aqueous solution (10 µM) of complex 2 at room temperature. The arrow indicates the increase of the complex concentration.

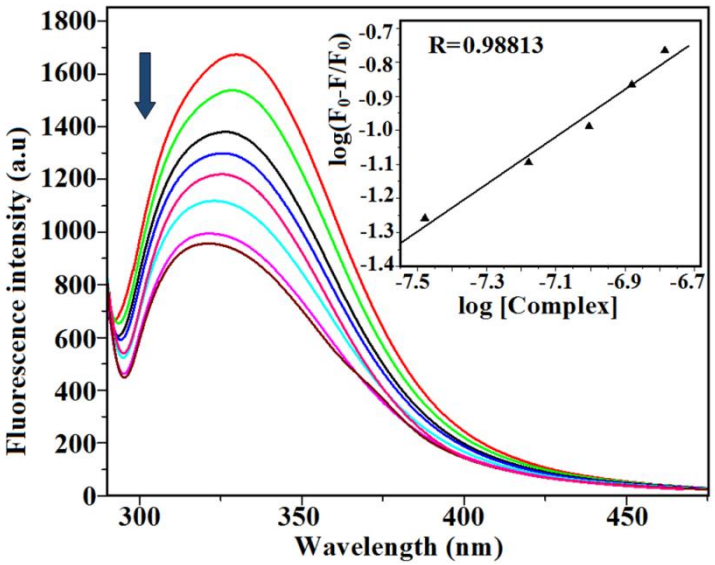

Figure 5.20. Change of the emission spectra of HSA (3 ml, 1.53 µM aqueous solution) upon gradual addition of 10 µL of an aqueous solution (10 µM) of complex 2 at room temperature. The arrow indicates the increase of the complex concentration.

Table 5.5. Kinetics parameters for the protein binding activities of the complexes 1 and 2.

Complex	k_b (L mol^{-1})	n	k_{sv}(L mol^{-1})	K_q(L mol^{-1}s^{-1})
1-BSA	$(4.21\times10^{7})\pm3.74$	(1.13 ± 0.08)	$(5.54\pm1.03)\times10^{6}$	$(5.54\pm1.03)\times10^{14}$
2-BSA	$(2.46\times10^{6})\pm2.31$	(1.02 ± 0.05)	$(1.54\pm0.12)\times10^{6}$	$(1.54\pm0.12)\times10^{14}$
1-HSA	$(8.53\times10^{3})\pm1.90$	(0.67 ± 0.03)	$(1.64\pm0.13)\times10^{6}$	$(1.64\pm0.13)\times10^{14}$
2-HSA	$(8.25\times10^{3})\pm2.76$	(0.66 ± 0.06)	$(1.26\pm0.04)\times10^{6}$	$(1.26\pm0.04)\times10^{14}$

The quenching of the fluorescence intensity of BSA and HSA solutions upon addition of the complexes is indicative of the association of serum albumins to the metal species. Fluorescence quenching may occur either by a static or dynamic mode. From the UV–Vis spectral study it was inferred that the absorption spectra of BSA/HSA are influenced by the addition of the complexes and the phenomenon evidenced the existence of a static interaction between the proteins and complexes studied.

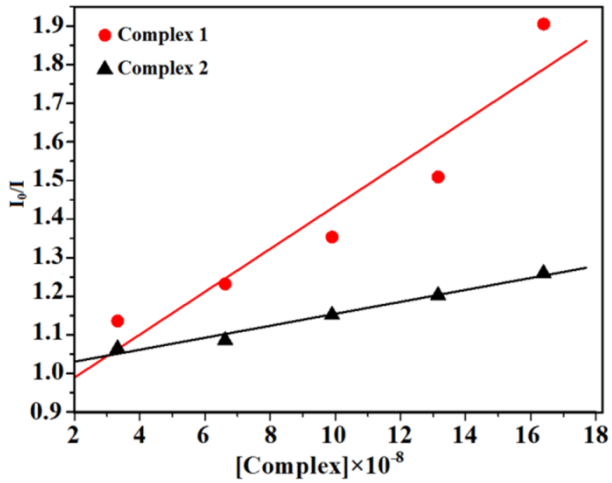

Figure 5.21. Stern-Volmer plot of complexes 1 and 2 with BSA.

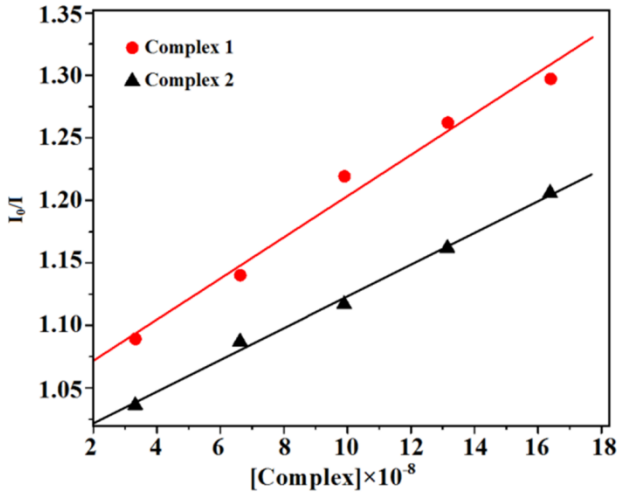

Figure 5.22. Stern-Volmer plot of complexes 1 and 2 with HSA.

5.3.7. DNA binding studies of the complexes

An aqueous solution of complex **1** showed bands at 229, 274 and 370 nm. Figure 5.23 shows the changes in the electronic absorption spectra of complex **1** upon gradual addition of 10 mL (6.66 mM) of an aqueous solution of CT-DNA to a 2 ml of complex aqueous solution (0.19 mM). The absorbance band at 274 nm gradually increased with a blue shift up to 269 nm (Figure 5.23). The isobestic points at 229, 241 and 348 nm in Figure 5.23 indicate the presence of more than two species in solution.[5.29] Complex **2** exhibited bands at 227, 273 and 364 nm, and those at 273 and 364 nm increased with a blue shift up to 270 and 350 nm, respectively (Figure 5.24), upon the gradual addition of the CT-DNA solution. The calculated

values of the intrinsic binding constant (K_{ib}) are 1.8×10^{6} and 1.1×10^{7} L mol^{-1} for **1** and **2**, respectively.

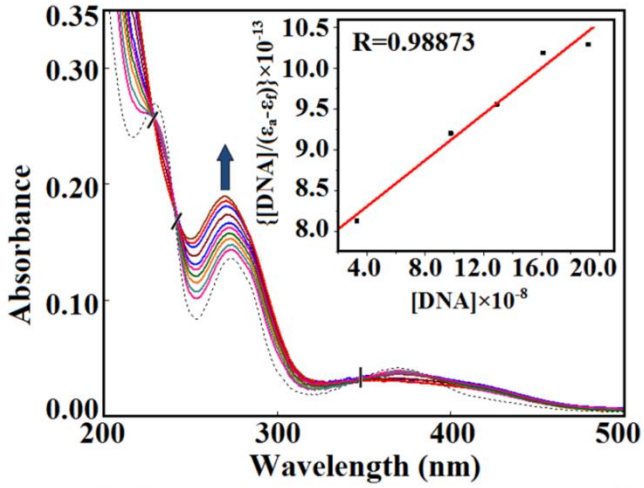

Figure 5.23. Change of the electronic absorption spectra of complex 1 (2 ml, 0.19 µM) upon the gradual addition of 10 µL of an aqueous solution (6.66 µM) of CT-DNA. Inset: Plot of [DNA] / (ε_a-ε_f) *vs* [DNA]. The arrow shows the changes in absorbance with the increase of DNA concentration.

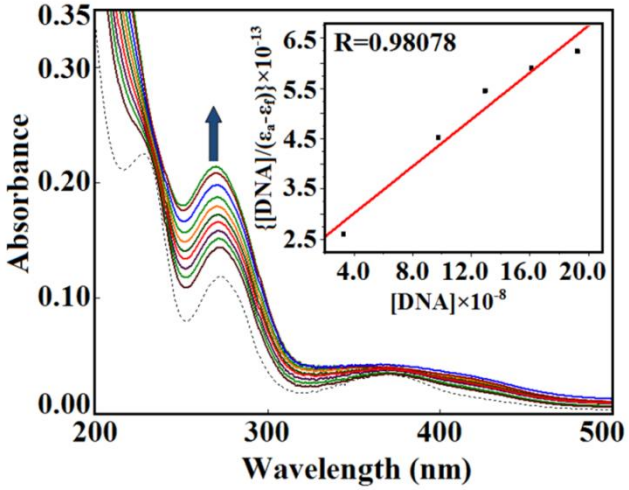

Figure 5.24. Change of the electronic absorption spectra of complex 2 (2 ml, 0.19 µM) upon the gradual addition of 10 µL of an aqueous solution (6.66 µM) of CT-DNA. Inset: Plot of [DNA] / (ε_a-ε_f) *vs* [DNA]. The arrow shows the changes in absorbance with the increase of DNA concentration.

Ethidium bromide (EtBr = 3,8-diamino-5-ethyl-6-phenylphenanthridinium bromide) shows fluorescence of an orange color when exposed to ultra violet radiation. EtBr bound to CT-DNA shows an emission band at 614 nm on excitation at 500 nm. Addition of a compound capable of interacting with CT-DNA results in quenching of the fluorescence intensity. In a fluorometric interaction study, a reduction of the fluorescence intensity was detected (Figures

5.25 and 5.26) upon gradual addition of 10 µL of a 10 µM aqueous solution of the complex to the aqueous solution of EtBr bound CT-DNA (2 ml 7.87 µM). This observation suggests that the complexes displaced EtBr molecules from the DNA binding sites. From the Stern–Volmer equation, linear relationships were obtained from the titration of EtBr–CT-DNA using the complexes as a quencher. The calculated values of the binding constant (K_{sv}) are 7.78×10^5 and 8.61×10^5 L mol^{-1} for **1** and **2**, respectively. The quenching of fluorescence occurs due to a decrease in the number of CT-DNA binding sites available for EtBr. The fluorescence quenching observed in the presence of the complexes may be due to intercalation of the complexes in the CT-DNA helices.

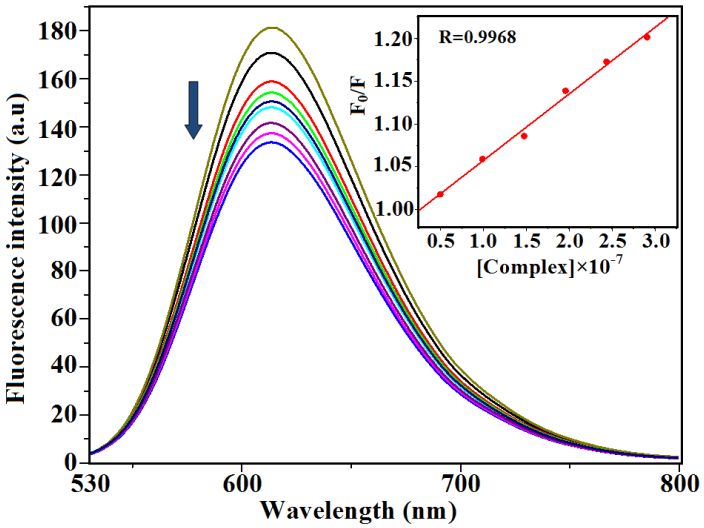

Figure 5.25. Fluorescence quenching curves of EB bound to CT-DNA upon gradual addition of complex 1 (10 µL, 10 µM). Inset: Stern-Volmer plot of the fluorescence titration.

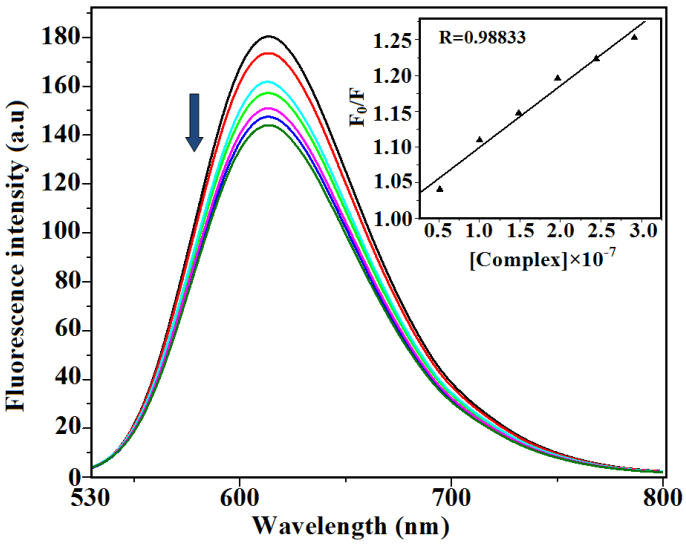

Figure 5.26. Fluorescence quenching curves of EB bound to CT-DNA upon gradual addition of complex 2 (10 µL, 10 µM). Inset: Stern-Volmer plot of the fluorescence titration.

5.3.8. Cyclic voltammetry studies

The electrochemical behavior of complexes **1** and **2** was investigated by cyclic voltammetry in methanol solution in the electric potential range from 0.0 to 0.6 V, using tetraethyl ammonium perchlorate (TEAM) as the supporting electrolyte (0.1 M). The cyclic voltammograms showed (Figure 5.27) an irreversible oxidation at 0.43 and 0.41 V for **1** and **2**, respectively, which was assigned to the Cu^{II}/Cu^{III} process.[5.30]

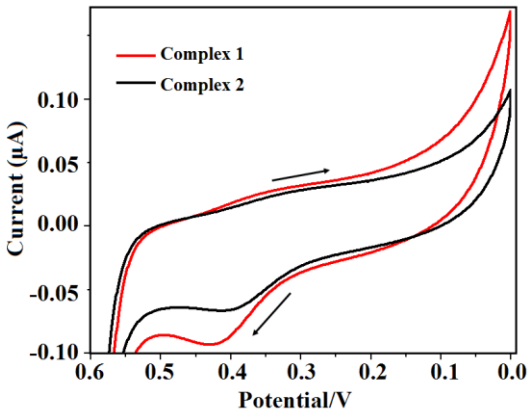

Figure 5.27. Cyclic voltammograms of complexes 1 and 2 (~1×10^{-3} M + 0.1 M NEt_4ClO_4). (Reference electrode: Ag/AgCl. Scan rate: 25 mV/s).

5.4. Conclusion

In summary, the synthesis, crystal structure, catecholase-like activity and study of the interactions with BSA/HSA and CT-DNA of two copper(II) compounds synthesized with 2-[(2-hydroxy-ethylimino)-methyl]-6-methoxy-phenol as a chelating ligand is reported here. Both compounds are tetranuclear with a double open cubane core structure. Electronic absorption and fluorescence spectroscopic studies indicate that both complexes interact with CT-DNA and serum albumins. In addition, complexes **1** and **2** are active towards the catalytic oxidation of 3,5-DTBC to 3,5-DTBQ in the presence of molecular oxygen, and **1** discloses a higher catalytic activity, likely induced by slightly different distortions of the copper center in comparison to **2**, or to templating effects of the counter ions.